Enhancing the chiroptical response of displaced overlapping perovskite metamaterials via compositional asymmetry

Yuyi Feng[1]*, Yuxuan Dong[1], Yifan Zeng[1], Hao Wang[1], Xin Bi[1], Shuxian Du[1], Yujie Qiu[1], Xianwen Liu[2], Jiajun Luo[3], Peng Cui[1], Xing Zhao[1], Meicheng Li[1]*

1. State Key Laboratory of Alternate Electrical Power System with Renewable Energy Sources, School of New Energy, North China Electric Power University, Beijing 102206, China
2. School of Optics and Photonics, Beijing Institute of Technology, Beijing, 100081, China
3. Sargent Joint Research Center, Wuhan National Laboratory for Optoelectronics and School of Optical and Electronic Information, Huazhong University of Science and Technology, Wuhan, 430074, China.

E-mail: yuyifeng@ncepu.edu.cn; mcli@ncepu.edu.cn

Abstract

Perovskite chiral metamaterials have shown great potential in applications such as circularly polarized light manipulation, information encryption, and biosensing. However, further enhancing their chiral optical performance remains a considerable challenge. Here, we propose a design strategy based on compositional asymmetry, introducing a $MAPbI_3/MAPbBr_3$ heterostructure into the two-wing architecture of a three-dimensional displaced perovskite metamaterial. This approach combines intrinsic material asymmetry with geometric asymmetry, enabling a synergistic enhancement of multiple chiral mechanisms. Experimental results reveal a notable circular dichroism (CD) response at 790 nm, with a peak absolute value of 21680 mdeg and an anisotropy factor (g-factor) as high as 1.37, significantly surpassing that of the homostructure control group. Further investigations demonstrate that adjusting the material composition of the heterostructure allows effective modulation of the peak wavelength and intensity of the CD signal at a fixed incident angle. This work provides a new pathway for tailoring chiroptical properties through chemical composition and broadens the application prospects of perovskite chiral metamaterials in multi-band circular polarization detection and encrypted optical devices.

1. Introduction

Chirality refers to the property of an object that cannot be perfectly superimposed with its mirror image through translation and rotation, which is a ubiquitous asymmetric phenomenon in nature[1]. In optics, chiral materials exhibit differential responses to left-handed circularly polarized light (LCP) and right-handed circularly polarized light (RCP),

Nano-optoelectronics and Micro/Nano-photonics XI, edited by Zhiping Zhou, Kazumi Wada, Shaoliang Yu, Proc. of SPIE Vol. 13723, 137230D · 2025 Published by SPIE
0277-786X · doi: 10.1117/12.3086762

thereby manifesting chiral optical effects such as circular dichroism (CD) and optical rotation. These effects have broad applications in optical imaging[2, 3], optical communication[4-6], information encryption[7, 8], and the detection of biological chiral molecules[9].

The chiral optical response of natural chiral materials is usually weak. However, by designing artificial micro-nano structures, such as G-shaped structures[10], helical lines[11, 12], and twisted nanorod pairs[13-15], chiral metamaterials can achieve optical chirality that is far greater than that of natural materials. In recent years, halide perovskite materials have become an ideal platform for the design of chiral metamaterials due to their excellent photoelectric properties, such as high absorption coefficient, long carrier diffusion length, and tunable band gap[16, 17].

The conventional method for endowing perovskite materials with chirality is to incorporate chiral organic molecules as components into the perovskite lattice, enabling the materials to acquire chirality through the transfer of chirality between molecules[17]. However, this method often leads to weak circular dichroism and a low anisotropy factor, making it challenging to satisfy the requirements of actual chiral photonic and spintronic devices. Furthermore, employing nanofabrication techniques such as electron beam lithography[18] to create perovskite metamaterials with chiral geometries can yield strong optical chirality. However, the high preparation costs and low efficiency associated with these methods limit their applicability in high-throughput fabrication. In our previous study, we designed a three-dimensional displaced overlapping structure perovskite metamaterial, inspired by classical helical chirality. We successfully fabricated this material through a stepwise inclined deposition technique. This approach not only results in strong chiral optical activity, but also meets the requirements of large-area and high-throughput fabrication. However, its chirality mainly originates from the geometrical asymmetry. How to further break through the optical chirality performance and obtain a more superior chiral optical response remains a major challenge. In 2018, Nechayev et al.[19] constructed a geometrically symmetric but material-asymmetric nanomaterial model composed of gold-silicon heterodimer. This study revealed that the inherent material heterogeneity, as a mechanism for breaking symmetry, can lead to significant circular dichroism and circular birefringence. In 2022, Wang et al.[20] used colloidal lithography technology to prepare arrays of gold-silver dual-metal hetero-nanohelmets. Their findings revealed that the introduction of hetero-metal materials generates a strong surface plasmon effect due to their differing dielectric constants and plasmon resonance characteristics. This approach achieved a g-factor of up to 0.26 in the visible light region.

Here, we propose a design strategy for incorporating multiple chirality into perovskite metamaterials. In a three-

dimensional displaced overlapping perovskite metamaterial with geometric asymmetry, a heteromaterial composed of two different perovskite materials is introduced, which enables the metamaterial to acquire compositional asymmetry, thereby enhancing the optical chirality.

This study designs a perovskite chiral metamaterial heterostructure and successfully fabricates a three-dimensional chiral perovskite metamaterial with a $MAPbI_3/MAPbBr_3$ heterostructure inside an anodic aluminum oxide (AAO) template using a sequential oblique evaporation and spin-coating method. Experimental results demonstrate that the hetero-structured chiral metamaterial exhibits a significantly enhanced circular dichroism (CD) response, with a maximum CD value reaching 21,680 mdeg and an anisotropy factor (g-factor) as high as 1.37.

2. Design principle and fabrication of three-dimensional heterogeneous structure perovskite chiral metamaterials

The three-dimensional displaced perovskite chiral metamaterial designed in this work is illustrated in Figure 1(a). The rotational symmetry is broken by a single wing-like structure, while the intrinsic mirror symmetry is further broken by the vertically displaced overlapping of two wings, thereby introducing strong chirality into the perovskite metamaterial. In this study, we extend this design by fabricating the two wings from distinct perovskite compositions. This material-level asymmetry, combined with the pre-existing geometric asymmetry of the displaced overlapping architecture, imparts multiple chiral mechanisms to the metamaterial. We performed finite-difference time-domain (FDTD) simulations to evaluate the optical performance of various material combinations within these metamaterials. As shown in Figure 1(b), the heterostructure configuration exhibits an approximately 72% enhancement in chiroptical response compared to its homogeneous counterparts. These simulation results are consistent with our assumptions. Guided by this principle, we successfully fabricated a three-dimensional displaced overlapping perovskite chiral metamaterial featuring compositionally distinct wings.

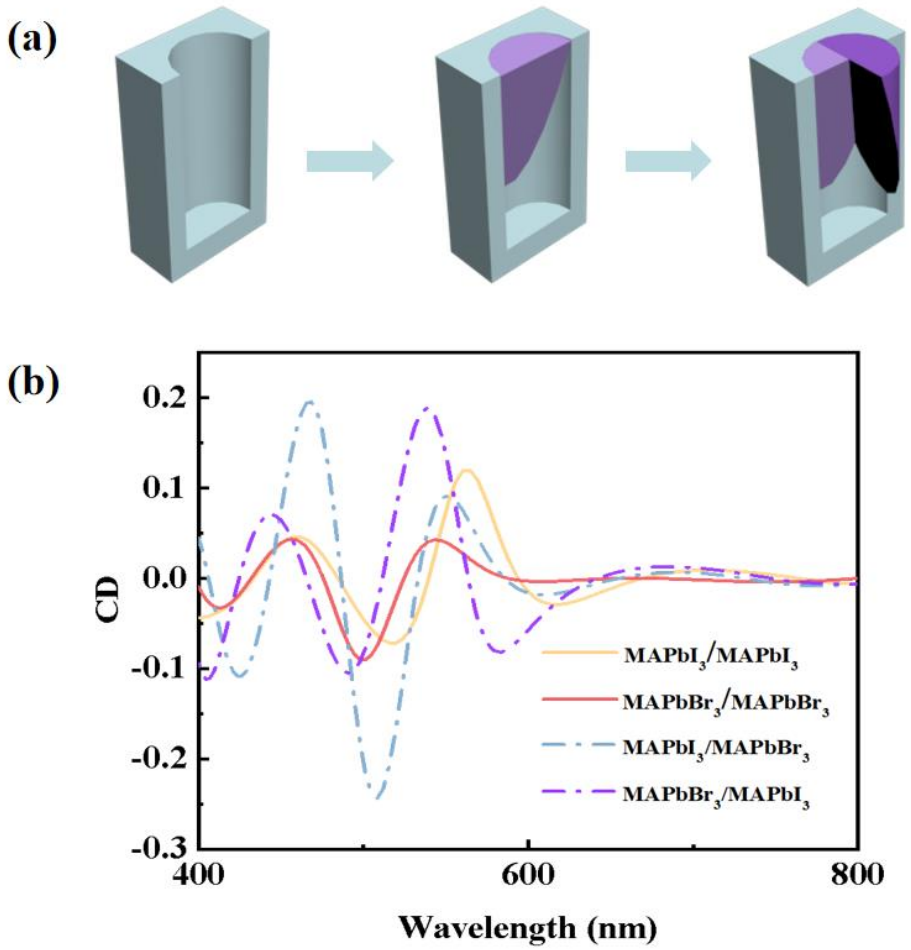

Figure 1. (a) Three-dimensional displaced overlapping perovskite chiral metamaterials design diagram; (b) Simulation CD diagrams corresponding to different component double-wing structures

This study utilizes a strategy combining anodic aluminum oxide (AAO) template-based sequential oblique-angle deposition with spin-coating methods to fabricate two distinct groups of three-dimensional chiral perovskite metamaterials featuring heterostructures. The fabrication procedure is schematically illustrated in Figure 2. The process began with the preparation of an AAO nanopore array on a silicon substrate[21]. Subsequently, the chiral heterostructures were constructed through multiple cycles of oblique thermal deposition and spin-coating. The initial deposition involved thermally evaporating PbI_2 into the AAO template at a 30° oblique incidence angle to form a primary precursor wing. This was followed by spin-coating methylammonium bromide (MABr) or methylammonium iodide (MAI) solutions onto the respective samples, which were subsequently annealed to convert the PbI_2 into $MAPbBrI_2$ or $MAPbI_3$ perovskite wings adhering to one side of the nanopores. To create the displaced overlapping dual-wing architecture and introduce

compositional asymmetry, the sample was rotated 90° clockwise within its plane. A second thermal deposition was then performed under identical conditions, introducing either PbI_2 or $PbBr_2$ as the precursor to form an asymmetrically stacked structure. Thereafter, the corresponding organic precursor solutions (MAI or MABr) were spin-coated again and annealed to form $MAPbI_3$ or $MAPbBr_3$ perovskite wings. This multi-step process ultimately yielded two groups of three-dimensional displaced overlapping perovskite chiral metamaterials with $MAPbBrI_2/MAPbI_3$ and $MAPbI_3/MAPbBr_3$ heterostructures, respectively.

As a control group, a homogeneous structured ($MAPbI_3/MAPbI_3$) chiral sample was fabricated by employing the identical fabrication procedure but using only PbI_2 for thermal deposition and MAI as the spin-coating solution.

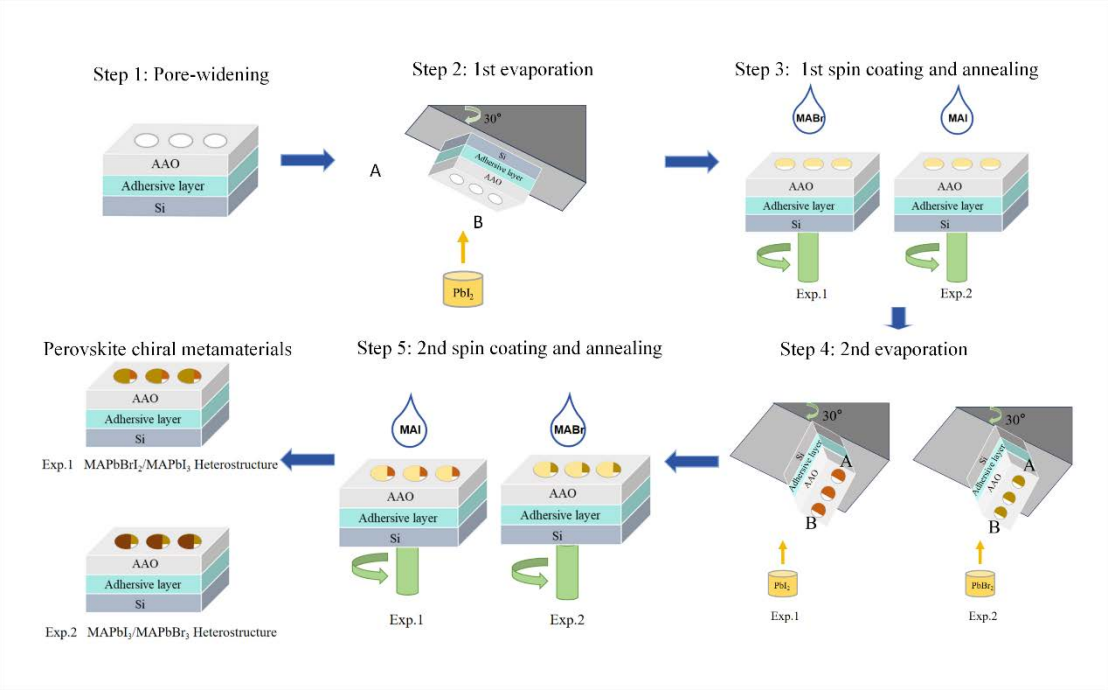

Figure 2. Fabrication of heterogeneous structure perovskite chiral metamaterial

3. Results and discussion

The reflection spectra of the two heterostructure samples ($MAPbBrI_2/MAPbI_3$ and $MAPbI_3/MAPbBr_3$) and the homogeneous control sample ($MAPbI_3/MAPbI_3$), measured under X- and Y-polarization at incident angles from 30° to 70°, are presented in Figure 3(a-c).

All three samples exhibited pronounced angular dependence and optical anisotropy. Taking the $MAPbI_3/MAPbBr_3$ heterostructure sample as an example (Figure 3c), the reflection spectra for X- and Y-polarized light were relatively close at a small incident angle (30°), suggesting weak anisotropy under this condition. As the incident angle increased to 70°,

the reflection spectrum for X-polarized light flattened and decreased in intensity, whereas that for Y-polarized light was enhanced. This evolution indicates a strong angular dependence in the optical response, demonstrating that larger incident angles effectively enhance the optical anisotropy. Notably, compared to the homogeneous control sample (Figure 3a), the heterostructure samples (Figure 3b-c) displayed a more distinct separation between X- and Y-polarizations in the long-wavelength range of 600-900 nm.

This pronounced angular-dependent anisotropy is further illustrated in the two-dimensional contour maps (Figure 3d-i). For the homogeneous $MAPbI_3/MAPbI_3$ structure under X-polarization excitation (Figure 3d), the reflection intensity around 580 nm gradually decreased with increasing incident angle. In contrast, under Y-polarization excitation (Figure 3g), the reflection intensity in the same spectral region increased significantly. This opposing trend reveals the intrinsic optical anisotropy of the metamaterials. Furthermore, the wavelength range of the anisotropic response flattened considerably with larger incident angles, almost covering a broad band from 400 to 900 nm at high angles of incidence (60°-70°). Regarding the $MAPbI_3/MAPbBr_3$ heterostructure sample, its overall reflection spectral line shape is similar to that of the $MAPbBrI_2/MAPbI_3$ heterostructure; however, it exhibits a lower reflectivity. This reduction can likely be attributed to a higher extinction coefficient of the surface film or increased interfacial scattering losses.

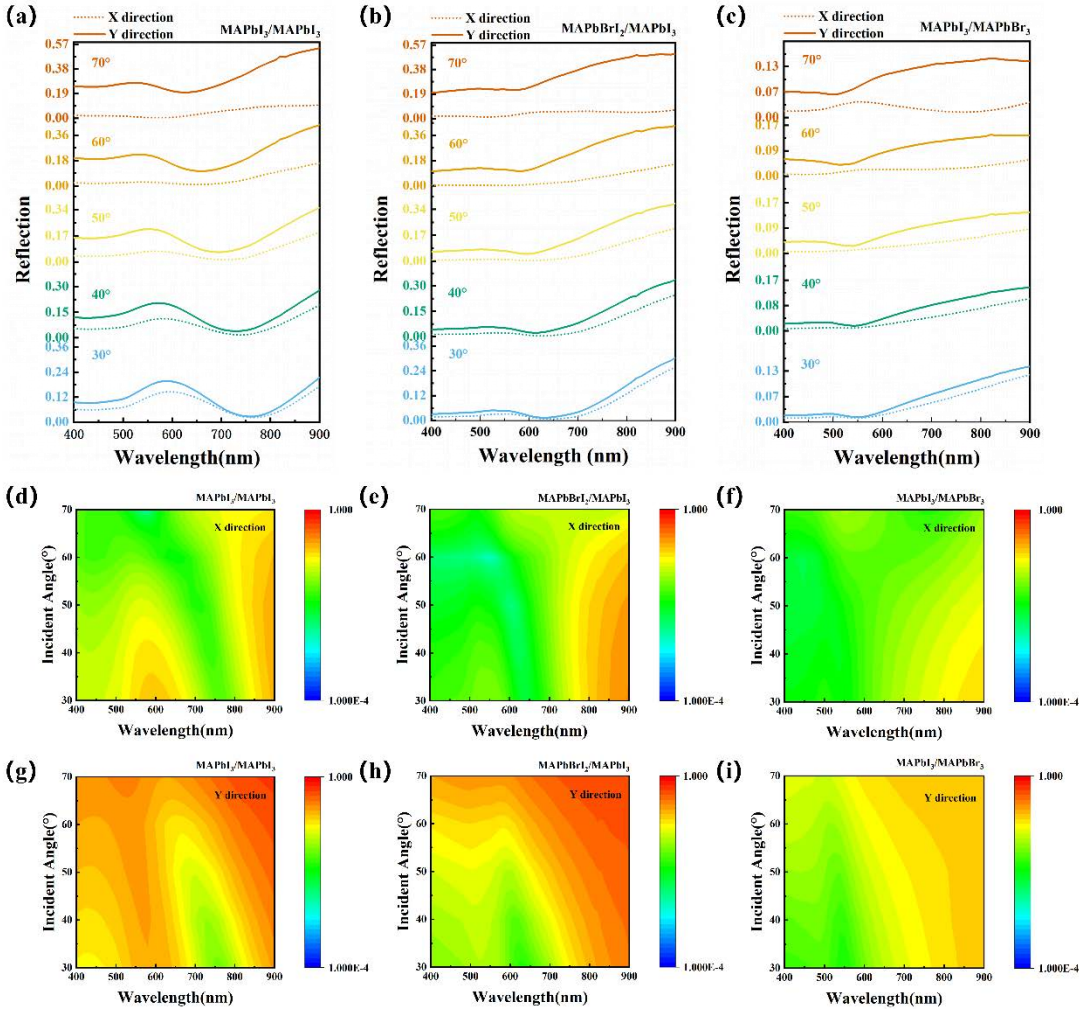

Figure 3. (a-c) Reflection spectra of the samples with different compositions under X- and Y-polarized light at various incident angles. (d-f) Contour plots of the reflection spectra under X-polarized illumination. (g-i) Contour plots of the corresponding spectra under Y-polarized illumination.

Subsequently, the complete set of ellipsometric parameters (Ψ, Δ) for the samples was obtained by using spectroscopic ellipsometry. The reflection CD was derived via Jones matrix analysis. The CD is defined as $CD = (R_{RCP} - R_{LCP}) / (R_{RCP} + R_{LCP})$, which represents the difference in reflection intensity between right- and left-handed circularly polarized light normalized by their sum. The anisotropy factor is defined as $g = 2(R_{RCP} - R_{LCP}) / (R_{RCP} + R_{LCP})$. Figure 4 presents the reflection spectra and their corresponding contour plots for the samples under circularly polarized light excitation at various incident angles.

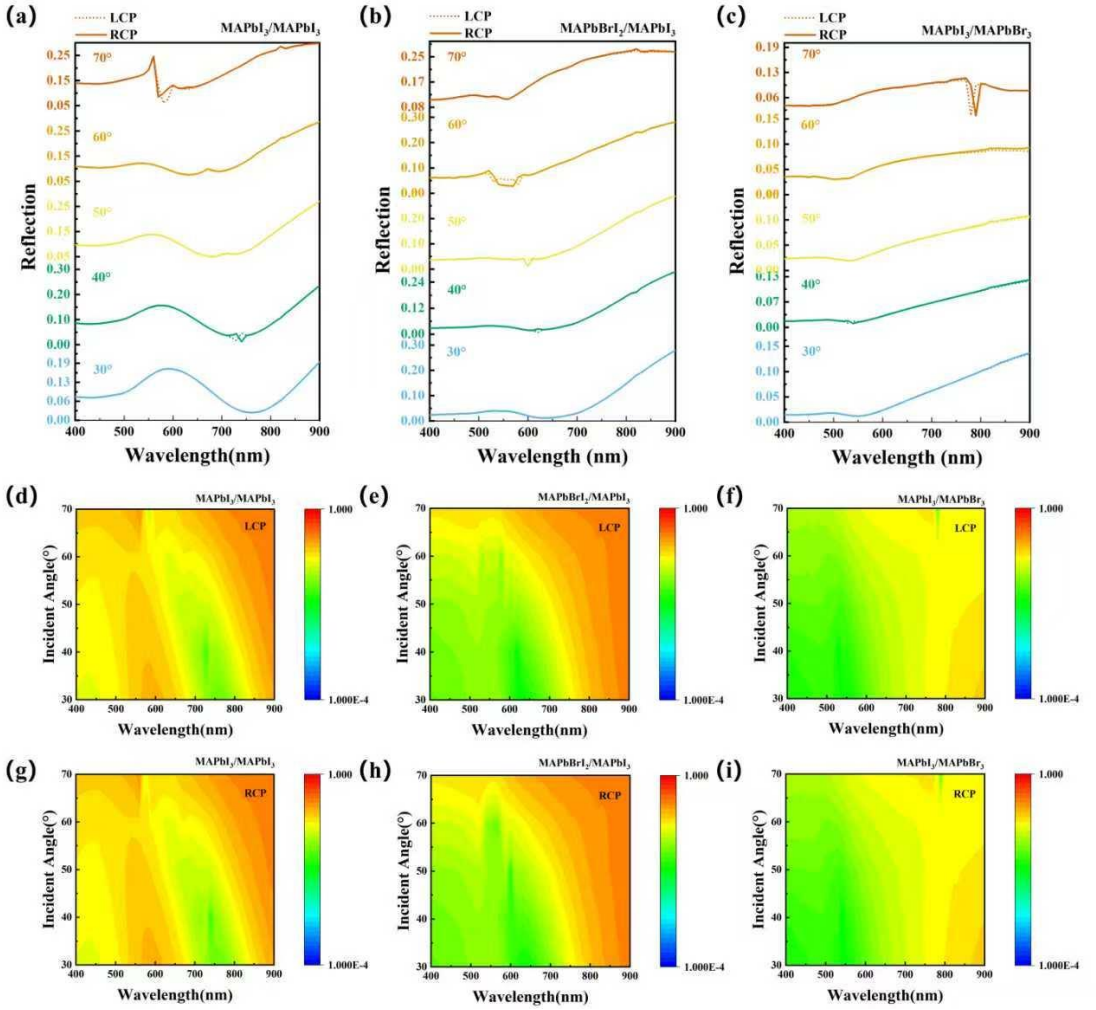

Figure 4. Experimental reflection spectra under circularly polarized light excitation. (a-c) Reflection spectra of the samples with different compositions under LCP and RCP light at various incident angles. (d-f) Contour plots of the reflection spectra under LCP excitation. (g-i) Contour plots of the reflection spectra under RCP excitation.

Figure 5 displays the reflection CD spectra and the corresponding contour plots for the samples with different compositions at various incident angles. For the homogeneous structure ($MAPbI_3/MAPbI_3$) at a 40° incident angle (Figure 5a), a sharp negative CD peak was observed around 740 nm, with an absolute value reaching 17,850 mdeg and a corresponding g-factor of 1.17. This result indicates that the displaced overlapping structure fabricated by oblique deposition can generate a significant chiroptical response. Notably, the CD signal exhibits a distinct bisignate feature, characterized by a positive shoulder adjacent to the main negative peak. This characteristic is typically attributed to the coupling between electric and magnetic dipole modes[16].

Upon introducing the heterostructure, the chiroptical response of the perovskite chiral metamaterial is significantly

enhanced. As shown in Figure 5e, the $MAPbI_3/MAPbBr_3$ heterostructure sample under a large incident angle of 70° generates a maximum CD response at 790 nm, with an absolute value reaching 21,680 mdeg and a substantially increased anisotropy factor (g) of 1.37. This result demonstrates that the heterostructure design successfully introduces compositional asymmetry into the displaced overlapping architecture, significantly enhancing the chiroptical activity of the metamaterials. Furthermore, the CD spectrum exhibits a strong positive peak at 780 nm, which, together with the negative peak at 790 nm, forms a clearly defined bisignate lineshape. This spectral feature strongly suggests the presence of enhanced coupling between electric and magnetic dipole modes within the heterostructure.

For the $MAPbBrI_2/MAPbI_3$ heterostructure sample, the strongest CD response occurred at an incident angle of 50° (Figure 5c), with the peak wavelength blueshifted to 600 nm. The maximum absolute CD value reached 16,230 mdeg, corresponding to a g-factor of 1.07. Compared to the homogeneous control sample, this heterostructure exhibited lower maximum CD signal and g-factor, along with the absence of a distinct bisignate feature. These observations may be attributed to interfacial defects and discontinuities introduced by the specific $MAPbBrI_2/MAPbI_3$ heterostructure design, which could lead to increased optical scattering and absorption. Furthermore, the less optimal matching of the optical properties between the constituent perovskite materials might have interfered with the chiral coupling resonance mode.

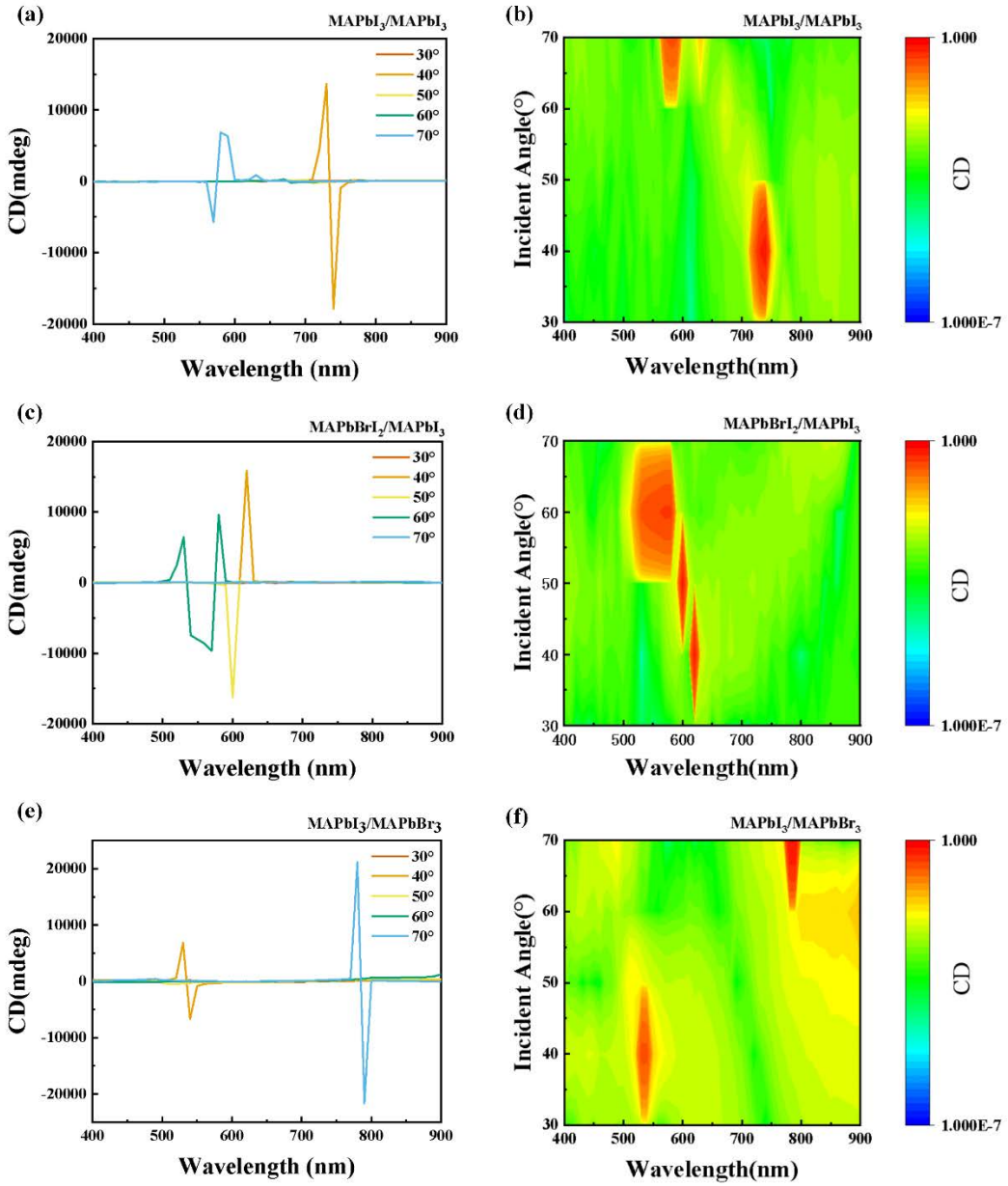

Figure 5. Circular dichroism (CD) response. (a, c, e) Reflection CD spectra of the samples with different compositions measured at various incident angles. (b, d, f) Contour plots of the CD spectra corresponding to (a, c, e), respectively.

It is noteworthy that all three perovskite chiral metamaterials exhibited significant chiroptical responses at an incident angle of 40°. As shown in Figure 6, the respective CD peaks were measured at 17,853 mdeg at 740 nm for $MAPbI_3/MAPbI_3$, 15,822 mdeg at 620 nm for $MAPbBrI_2/MAPbI_3$, and 6,837 mdeg at 530 nm for $MAPbI_3/MAPbBr_3$. These results demonstrate that the CD peak wavelength of the displaced overlapping perovskite chiral metamaterial can be effectively tuned across different spectral regions by modifying the chemical composition of the two constituent wings, while

maintaining a fixed 40° incidence angle.

The energy band structure of the heterostructure likely influences the resonance wavelength of its chiroptical response. The band gaps of $MAPbI_3$, $MAPbBrI_2$, and $MAPbBr_3$ increase sequentially ($MAPbI_3 < MAPbBrI_2 < MAPbBr_3$)[22], leading to a corresponding increase in the intrinsic energy of their optical transitions (i.e., a blueshift in wavelength). The CD response of the heterostructure results from the synergistic interplay between the geometric chirality and the intrinsic optical properties of the constituent materials. Consequently, as the intrinsic absorption edge of the material blueshifts with increasing bromine content, the peak wavelength of the chiral resonance also undergoes a blueshift. The variation in signal intensity is associated with the absorption coefficient, refractive index of the materials at specific wavelengths, and the quality of the heterojunction interface.

Therefore, by varying the heterostructure combinations within the perovskite chiral metamaterials, the peak wavelength and intensity of its chiroptical response can be actively modulated at a fixed incident angle. This strategy reveals a novel pathway for tuning chiroptic properties through chemical composition, demonstrating significant potential for applications in multi-spectral circularly polarized light detection and chiral information encryption.

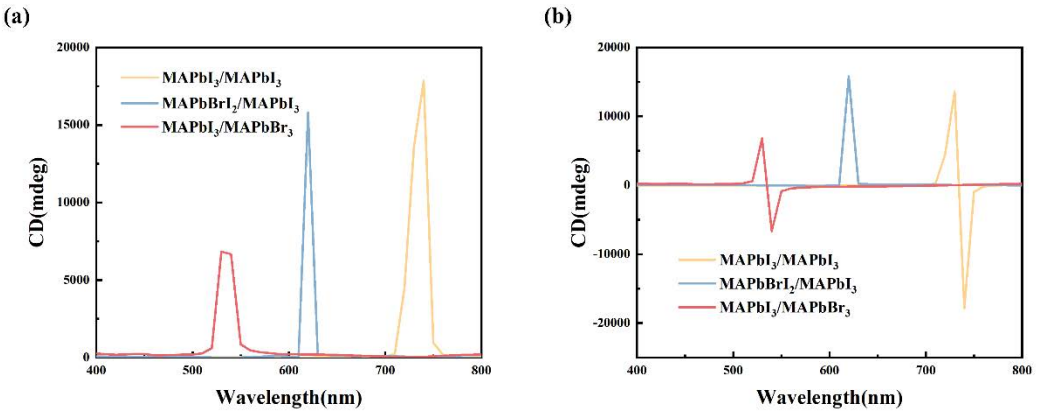

Figure 6. Reflection circular dichroism (CD) spectra at an incident angle of 40°. (a) Spectra of the absolute CD values. (b) The corresponding signed CD spectra.

4. Conclusion

In summary, this study proposes a design strategy for incorporating multifunctional chirality into perovskite metamaterials. By introducing a heterostructure composed of two distinct perovskite materials into a three-dimensional displaced overlapping architecture with inherent geometric asymmetry, we have successfully integrated compositional asymmetry into the metamaterial system. Both simulation and experimental results confirm that this heterostructure design

effectively combines compositional asymmetry with the pre-existing structural asymmetry, leading to a significant enhancement of the chiroptical response. The fabricated $MAPbI_3$/$MAPbBr_3$ heterostructure sample exhibited a remarkably strong CD response of 21,680 mdeg at 790 nm under 70° incidence, achieving a giant anisotropy factor (g-factor) of 1.37. Furthermore, at a fixed incident angle, actively tuning the heterojunction combination within the displaced overlapping perovskite chiral metamaterial allows for precise modulation of the peak wavelength and intensity of the chiroptical response. This work unveils a novel pathway for manipulating chiroptical properties through chemical composition engineering, demonstrating considerable potential for applications in advanced photonic devices.

Acknowledgments

This work is supported partially by National Natural Science Foundation of China (62405088).

Reference

[1]Yiqiao Tang and Adam E. Cohen, "Optical chirality and its interaction with matter," Phys. Rev. Lett. 104, 163901 (19 April 2010).https://journals.aps.org/prl/abstract/10.1103/PhysRevLett.104.163901

[2]Sean P. Rodrigues, et al., "Nonlinear imaging and spectroscopy of chiral metamaterials," Adv. Mater. 26(35), 6157-6162 (17 September 2014).https://advanced.onlinelibrary.wiley.com/doi/full/10.1002/adma.201402293

[3]M. Khorasaninejad, et al., "Multispectral chiral imaging with a metalens," Nano Lett. 16(7), 4595–4600 (7 June 2016).https://pubs.acs.org/doi/full/10.1021/acs.nanolett.6b01897

[4]Peng Chen, et al., "Chirality invertible superstructure mediated active planar optics," Nat Commun 10, 2518 (07 June 2019).https://doi.org/10.1038/s41467-019-10538-w

[5]Peter Lodahl, et al., "Chiral quantum optics," Nature 541, 473–480 (26 January 2017). https://doi.org/10.1038/nature21037

[6]Shengyan Yang, et al., "Spin-selective transmission in 3D chiral folded metasurfaces," Nano Letters 19(6), 3432–3439 (4 January 2019).https://doi.org/10.1021/acs.nanolett.8b04521

[7]Yoon Ho Lee, et al., "Hierarchically manufactured chiral plasmonic nanostructures with gigantic chirality for polarized emission and information encryption," Nat Commun 14, 7298 (10 November 2023).https://doi.org/10.1038/s41467-023-43112-6

[8]Sufan Li, et al., "Dynamic optical chirality based on liquidcrystal-embedded nano-cilia photonic structures," Nat Commun 16, 6569 (17 July 2025).https://doi.org/10.1038/s41467-025-61982-w

[9]Maryam Hajji, et al., "A chiral quantum metamaterial for hypersensitive biomolecule detection," ACS Nano 15(12), 19905–19916 (30 November 2021).https://doi.org/10.1021/acsnano.1c07408

[10]Evgeniy Mamonov, et al., "Circular dichroism in optical second harmonic generated in reflection from chiral G-shaped metamaterials," J. Phys.: Conf. Ser. 352, 012029 (2012).https://iopscience.iop.org/article/10.1088/1742-6596/352/1/012029/meta

[11]Ufuk Kilic, et al., "Broadband enhanced chirality with tunable response in hybrid plasmonic helical metamaterials," Adv. Funct. Mater. 31, 2010329 (17 February 2021).https://doi.org/10.1002/adfm.202010329
[12]Davey C. Hoekstra Augustinus J. J. Kragt, et al., "3D helix engineering in chiral photonic materials," Adv. Mater. 31, 1903120 (27 June 2019).https://doi.org/10.1002/adma.201903120
[13]Nicholas A. Kotov, et al., "Chiral nanostructures: new twists," ACS Nano 15(8), 12457–12460 (24 August 2021).https://doi.org/10.1021/acsnano.1c06959
[14]JIANXING ZHAO, et al., "Optical chirality breaking in a bilayered chiral metamaterial," Opt. Express 25, 23051-23059 (18 September 2017).https://doi.org/10.1364/OE.25.023051
[15]Y. Zhao, et al., "Twisted optical metamaterials for planarized ultrathin broadband circular polarizers," Nat Commun 3, 870 (29 May 2012).https://doi.org/10.1038/ncomms1877
[16]Guankui Long, et al., "Perovskite metasurfaces with large superstructural chirality," Nat Commun 13, 1551 (23 March 2022).https://doi.org/10.1038/s41467-022-29253-0
[17]Guankui Long, et al., "Chiral perovskite optoelectronics," Nat Rev Mater 5, 423–439 (10 March 2020).https://doi.org/10.1038/s41578-020-0181-5
[18]Jose Mendoza-Carreño, et al., "Nanoimprinted 2D-chiral perovskite nanocrystal metasurfaces for circularly polarized photoluminescence," Adv. Mater. 35, 2210477 (19 January 2023).https://doi.org/10.1002/adma.202210477
[19]Sergey Nechayev, et al., "Mirror-symmetric heterogeneous resonant nanostructures: extrinsic chirality and spin-polarized scattering," Laser & Photonics Reviews 12, 1800109 (30 July 2018).https://doi.org/10.1002/lpor.201800109
[20]Yu Wang, et al., "Chiral nanohelmet array films with three-dimensional (3D) resonance cavities," J. Colloid Interface Sci. 626, 334-344 (15 November 2022).https://doi.org/10.1016/j.jcis.2022.06.160
[21]Y. Feng, et al., "Giant polarization anisotropic optical response from anodic aluminum oxide templates embedded with plasmonic metamaterials," Optics Express 28(20),29513-29528 (28 September 2020).https://doi.org/10.1364/OE.403437
[22]Md Jakaria Talukder, et al., "Advances in high-efficiency solar photovoltaic materials: a comprehensive review of perovskite and tandem cell technologies," AJATES 1 (01), 201-225. (3 February 2025).https://doi.org/10.63125/5amnvb37